International Journal of Thermophysics, Vol. 14, No. 6, 1993

Application of Photoacoustic and Photothermal Techniques for Heat Conduction Measurements in a Free-Standing Chemical Vapor-Deposited Diamond Film

C. Glorieux,[1] J. De Groote,[1] J. Fivez,[1,2] W. Lauriks,[1] and J. Thoen[1]

Received May 4, 1993

Heat conduction in a free-standing chemical vapor-deposited polycristalline diamond film has been investigated by means of combined front and rear photoacoustic signal detection techniques and also by means of a "mirage" photothermal beam deflection technique. The results obtained with the different techniques are consistent with a value of $\alpha = (5.5 \pm 0.4) \times 10^{-4}\ m^2 \cdot s^{-1}$ for thermal diffusivity, resulting in a value of $\kappa = (9.8 \pm 0.7) \times 10^2\ W \cdot m^{-1} \cdot K^{-1}$ for thermal conductivity when literature values for the density and heat capacity for natural diamond are used.

KEY WORDS: chemical vapor-deposited diamond film; heat conduction; mirage effect; photoacoustics; thermal conductivity; thermal diffusivity.

1. INTRODUCTION

Diamond has many unique physical properties, e.g., chemical and thermal stability, optical transparency over a wide range of frequencies, hardness, and high thermal conductivity, which makes it of special importance for many technological applications. In fact, diamond is known to have a higher thermal conductivity, κ, at room temperature, than any other known substance, ranging from about 1000 to more than 2000 $W \cdot m^{-1} \cdot K^{-1}$, depending on the sample origin. Thin films grown by

[1] Laboratorium voor Akoestiek en Warmtegeleiding, Departement Natuurkunde, Katholieke Universiteit Leuven, Celestijnenlaan 200D, B-3001 Leuven, Belgium.

[2] EHSAL, Stormstraat 2, B-1000 Brussel, and Universitaire Faculteiten St. Ignatius, Faculteit TEW, Prinsstraat 13, B-2000 Antwerpen, Belgium.

840/14/6-7

chemical vapor deposition (CVD) usually fall around the lower end of this range.

In the case of CVD diamond samples, the high thermal conductivity and the thin-film geometry pose special limitations on the measuring techniques in order to arrive at a reliable thermal conductivity value. As in the case of natural diamond samples, both static and dynamic methods have been applied to thin diamond films. Steady-state techniques have been used by Morelli et al. [1] and by Ono et al. [2]. In the former case, the temperature profile across the film was measured with a four-probe technique. In the latter case, it was recorded by an infrared thermograph. Dynamic methods for measuring heat conduction in diamond films have been used by Kuo et al. [3, 4], Albin et al. [5], and Visser et al. [6]. Kuo et al. [3, 4] used a photothermal beam deflection technique, or "mirage" technique, to probe surface temperature fluctuations of the sample. Albin et al. [4] used a heat pulse technique to induce thermal waves in a sample and surface temperatures were recorded by an infrared scanner. An infrared technique was also used for diamond films by Visser and co-workers [6].

In this paper, we present results for a free-standing CVD polycrystalline diamond film obtained by two different measuring techniques: a combination of a front and rear photoacoustic detection technique and a "mirage" beam deflection technique. The latter method is very similar to the one also used by Kuo et al. [3, 4]. Because of the rather complicated expression (see further) for the photoacoustic (PA) signal with a substantial amount of difficult to determine setup dependent parameters, it is common practice to do relative measurements by calibrating with a reference material, for which quite often carbon is used [7, 8]. In some experiments the reference material is enclosed with the sample in the PA cell, allowing the generation of a PA signal by the sample or the reference without disturbing the cell characteristics. Moreover, one can select a reference material which is very similar to the sample [9, 10]. For samples which have a large optical absorption coefficient, one can avoid a reference material altogether by combining the photoacoustic signals generated at the front surface and the rear surface of the sample, provided one chooses the proper modulation frequency regime (i.e., the sample should not be completely thermally thick). This approach was introduced by Yasa and Amer [11], who have combined the amplitude of the rear-surface illuminated signal with the amplitude of the front-surface illuminated signal. In a similar approach Pessoa et al. [12] proposed a method in which the relative phase lag between the front and the rear signal at a given modulation frequency was used. In our approach we also combine the front and rear signals, but we use the complete amplitude and phase data of the signal for several modulation frequencies. By means of a simultaneous nonlinear least-

squares fitting procedure, we are thus able to extract fully the information on the sample present in the PA signal.

In the photoacoustic technique we probe heat conduction across the shortest sample dimension, while in the "mirage" technique we measure heat flow in the plane of the film. For polycrystalline samples values obtained for the thermal conductivity should of course be the same. However, for anisotropic materials a combination of both methods could be used to reveal differences in thermal conductivity.

2. EXPERIMENTAL TECHNIQUES

2.1. Photoacoustic Microphone-Detection Technique

In a photoacoustic experiment investigating condensed matter, the signal is caused by that fraction of the modulated optical energy which is converted to heat in the sample via nonradiative deexcitation processes. The periodic absorption of light produces a fast-decaying thermal wave in the sample but also generates an acoustical wave by the local expansion and contraction of the sample due to the periodic heating. In a general description both types of waves have to be considered [13, 14]. In a broad range of situations the contribution of the acoustical wave can be neglected and one has to consider only the thermal wave. By properly choosing the experimental configuration, the one-dimensional model of Rosencwaig and Gersho (RG) [15] can be used. In a typical photoacoustic setup the sample is placed in a closed cell containing a gas (e.g., air) and illuminated with modulated (chopped) laser light, which is absorbed by the sample. In the RG model one assumes the light intensity to be uniform across the sample, resulting in an amplitude of the thermal source depending only on the depth in the sample and decaying exponentially with the distance from the surface.

In Fig. 1, a very schematic cross-sectional view of a photoacoustic cell and relevant coordinates for the one-dimensional model are given. A microphone detector in contact with the cell gas (through an opening in the cell wall) has been omitted.

If one assumes the incident monochromatic light, at the wavelength λ, to be sinusoidally modulated, the following result holds for the heat density produced at any point x in the sample due to light absorbed at that point.

$$H(x) = (\tfrac{1}{2})\,\beta_s(\lambda)\, I_0(\lambda)(1 + \cos \omega t) \exp \beta_s(\lambda) x \tag{1}$$

with I_0 the incident intensity, β_s the optical absorption coefficient of the sample, and $f = \omega/2\pi$ the modulation frequency. In Fig. 1 the x values of

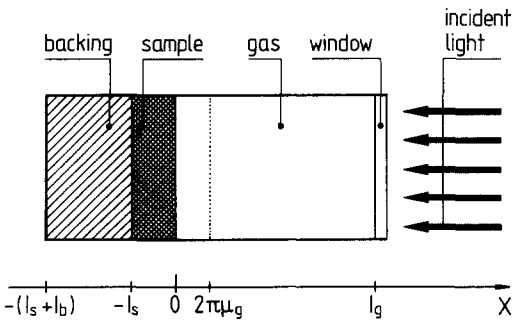

Fig. 1. Schematic cross-sectional view of a simple cylindrical photoacoustic cell, showing coordinates relevant for the one-dimensional model.

Eq. (1) range from $x=0$ at the gas–sample interface to $x=-l_s$ at the sample backing interface. The gas column extends from $x=0$ to $x=l_g$ and the backing material to $-(l_s+l_b)$.

On the basis of thermal diffusion equations for the gas, the sample, and the backing (including a distributed heat source for the sample only) and suitable boundary conditions (continuity of temperature and heat flux), Rosencwaig and Gersho [15] arrived at the following expression for the complex amplitude θ_f of the periodic temperature at the sample–gas (front) interface ($x=0$):

$$\theta_f = E\left[\frac{(r-1)(b+1)\,e^{\sigma_s l_s}-(r+1)(b-1)\,e^{-\sigma_s l_s}+2(b-r)\,e^{-\beta_s l_s}}{(g+1)(b+1)\,e^{\sigma_s l_s}-(g-1)(b-1)\,e^{-\sigma_s l_s}}\right] \tag{2}$$

with $E=\eta\beta_s I_0/[2\kappa_s(\beta_s^2-\sigma_s^2)]$. In this expression κ_s is the thermal conductivity of the sample, η the photothermal conversion efficiency, $\sigma_s=(1+i)\,a_s$, with a_s the thermal diffusion coefficient equal to the inverse of the thermal diffusion length $\mu_s=(2\alpha_s/\omega)^{1/2}$ of the sample. $\alpha_s=\kappa_s/(\rho_s C_s)$ is the sample thermal diffusivity, with ρ_s its density and C_s its heat capacity (per unit mass). One further has $r=(1-i)\beta_s/(2a_s)$, $b=\kappa_b a_b/(\kappa_s a_s)$, and $g=\kappa_g a_g/(\kappa_s a_s)$. The subscripts s, b, and g refer to the sample, the backing material, and the cell gas, respectively.

Only a relatively thin layer of gas ($\simeq 2\pi\mu_g$) adjacent to the front surface of the sample will be affected by the periodic temperature variations given by θ_f in Eq. (2). This boundary layer of gas can then be considered as a thermal piston creating the acoustical signal detected by the microphone in the cell wall. The pressure variation, δP, in the gas is obtained by assuming an adiabatic response to the piston [15]. Further, it is also assumed that l_g is much smaller than the acoustical wavelength for

the modulation frequency $f = \omega/2\pi$. The following result can then be derived [15]:

$$\delta P_f = Q_f \exp(i\omega t - i\pi/4) \tag{3}$$

where

$$Q_f = \frac{\gamma_g P_0 \theta_f}{(2)^{1/2} T_0 l_g a_g} = q_f e^{-i\psi_f} \tag{4}$$

with P_0 and T_0 the cell pressure and temperature and γ_g the ratio of the specific heats at a constant pressure and constant volume of the gas.

If the sample is thermally sufficiently thin ($l_s < 2\pi\mu_s$), there will also be a periodic temperature variation at the sample backing interface, which we can indicate as the rear thermal signal θ_r. It is possible to arrive at an expression for θ_r in terms of the sample, backing, and gas properties as well. Infact, recently we have reported [16] an extension for a k-layer system, allowing the derivation of the periodic temperature variation at each interface between layers, including the interface between the $(k-1)$th layer and an infinitely thermally thick kth backing layer. Applying that procedure to the situation considered here, we arrive at the following expression for θ_r:

$$\theta_r = E\left[\frac{(g-1)(r-1)\,e^{-(\beta_s+\sigma_s)l_s} - (g+1)(r+1)\,e^{-(\beta_s-\sigma_s)l_s} + 2(r+g)}{(g+1)(b+1)\,e^{\sigma_s l_s} - (g-1)(b-1)^{-\sigma_s l_s}}\right] \tag{5}$$

In Section 3, we show how a combination of Eqs. (2) and (5) for θ_f and θ_r for a free-standing film with the same gas on both sides results in a convenient procedure for arriving at the thermal parameters of the sample.

2.2. Photothermal Beam-Deflection Detection Technique

The second method which we have applied to probe a free-standing CVD film is photothermal beam deflection, or the so-called "mirage" detection technique. This technique has become well established since its introduction around 1980 by Boccara et al. [17]. We use a version of this technique in which the pump laser beam is focused on the surface of the sample in order to create a localised heat source and hence to launch a thermal wave in the solid sample and the surrounding air. A second probe laser beam parallel to the sample surface is used to detect the temperature gradient in the air just above the surface as a function of distance from the localized heat source. In Fig. 2, a schematic representation of the

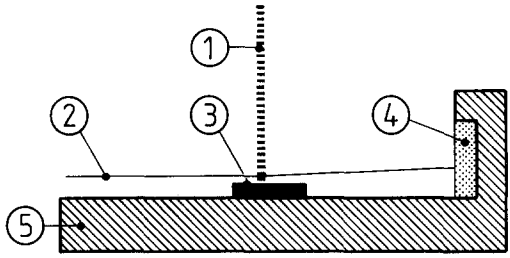

Fig. 2. Schematic view of a photothermal beam deflection setup, with (1) the modulated pump beam, (2) the probe beam, (3) the sample, (4) the position sensitive detector, and (5) the background material.

experimental setup is given. If the harmonically modulated pump beam is sufficiently focused and the thermal diffusion length μ_s of the sample is substantially larger than the sample thickness l_s, one can consider the model geometry as that of a harmonic point source in an infinite, two-dimensional sheet with in-plane heat transport in the sample only. For the specific case of a continuous, harmonic heat source $h(t) = h_0 \exp[i\omega t]$, the pump beam along the z axis and the heat transport in the (x, y)-plane, one has for the complex periodic temperature variation [6, 18]

$$T_c = \frac{h_0 e^{i\omega t}}{2\pi\kappa_s} K_0[(i\omega/\alpha_s)^{1/2} r] \tag{6}$$

with $r = (x^2 + y^2)^{1/2}$ the distance from the point source and $K_0[(i\omega/\alpha_s)^{1/2} r]$ the modified Bessel function of the second kind of order zero. The periodic temperature variation of the sample surface will result in a thermal wave in the gas propagating in the z direction. In the same way as in the photoacoustic treatment [15], one arrives at the following result:

$$T_g = T_c e^{-\sigma_g z} \tag{7}$$

Because of the resulting periodic temperature variation in the gas above the sample surface, there will also be a periodically changing refractive index (n) gradient, which in turn will produce an periodic deflection of the probe beam (see Fig. 2) parallel to the sample surface. In order to arrive at the deflection of the test beam, one has to integrate along the path of the beam. Assuming the probe beam directed along the x direction, one has [19, 20] the following expressions for the transverse and the normal components of the deflection:

$$\varphi_t = \frac{1}{n}\frac{dn}{dT}\int_{y=-\infty}^{\infty} \frac{\partial T_g}{\partial x}\, dy \tag{8}$$

$$\varphi_n = \frac{1}{n}\frac{dn}{dT}\int_{y=-\infty}^{\infty} \frac{\partial T_g}{\partial z}\, dy \tag{9}$$

Combination of Eqs. (8) and (9) with Eqs. (7) and (6) results in

$$\varphi_t(x) = \frac{1}{n}\frac{dn}{dT}\frac{h_0}{2\pi\kappa_s} e^{-\sigma_g z_0} e^{i\omega t} \int_{y=-\infty}^{\infty} \frac{\partial K_0[(i\omega/\alpha_s)^{1/2} r]}{\partial x}\, dy \tag{10}$$

$$\varphi_n(x) = -\frac{1}{n}\frac{dn}{dT}\frac{h_0\sigma_g}{2\pi\kappa_s} e^{-\sigma_g z_0} e^{i\omega t} \int_{y=-\infty}^{\infty} K_0[(i\omega/\alpha_s)^{1/2} r]\, dy \tag{11}$$

3. EXPERIMENTAL RESULTS AND DISCUSSION

3.1. Photoacoustic Measurements

We have carried out a series of photoacoustic measurements on a polycrystalline CVD diamond film of the same origin as the sample used by Visser et al. [6], with a thickness $l_s = 315\ \mu$m. In order to increase the photoacoustic signal the sample was coated with a thin layer of Ti with a low reflectivity. As a periodic heat source a chopped argon ion laser with a power of 1 W (all lines) was used. The microphone signal was measured by means of a lock-in amplifier.

In principle it is possible to arrive, on the basis of Eqs. (2) to (4), at the thermal parameters of a given sample. This, however, demands sufficient knowledge of thermal parameters of the gas and the backing as well as of optical parameters (η and β_s) of the sample itself or of the applied coating. Moreover, the relationship between the measured microphone signal and the PA signal can be rather complicated: the photoacoustic cell, the microphone, the amplifiers, and the filters do not have a flat frequency response. Therefore, one needs a calibration procedure. This is possible using a reference material with known thermal and optical properties. The measured (index m) amplitude A and phase ψ of the sample and reference signal can be written as

$$A^m_{\text{sample}} = A_{\text{sample}} \times f_{\text{sys}} \tag{12}$$

$$\psi^m_{\text{sample}} = \psi_{\text{sample}} + \psi_{\text{sys}} \tag{13}$$

$$A^m_{\text{ref}} = A_{\text{ref}} \times f_{\text{sys}} \tag{14}$$

$$\psi^m_{\text{ref}} = \psi_{\text{ref}} + \psi_{\text{sys}} \tag{15}$$

The latter two equations yield the system response (f_{sys}, ψ_{sys}), which can be used to solve A_{sample} and ψ_{sample} in the former two equations.

It is, however, also possible to avoid the use of a reference material by a proper combination of the rear and front signals for thermally sufficiently thin samples. Indeed from Eqs. (2) and (5) one sees that the denominator and the prefactor E are the same provided one uses as backing material the same gas as in front of the sample. In this situation, one obtains for the ratio of the two complex microphone signals the following expression:

$$Q=\frac{Q_r}{Q_f}=\frac{\theta_r}{\theta_f}$$
$$=\frac{(g-1)(r-1)\,e^{-(\beta_s+\sigma_s)l_s}-(g+1)(r+1)\,e^{-(\beta_s-\sigma_s)l_s}+2(r+g)}{(r-1)(b+1)\,e^{\sigma_s l_s}-(r+1)(b-1)\,e^{-\sigma_s l_s}+2(b-r)\,e^{-\beta_s l_s}} \tag{16}$$

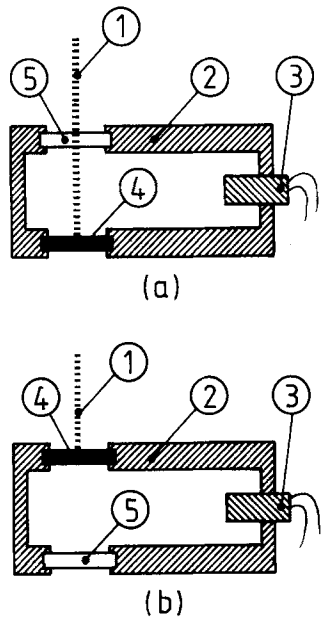

Fig. 3. Schematic diagram of the photoacoustic measuring cell in the front (a) and rear (b) detection configuration. (1) The modulated laser beam; (2) the cell body; (3) the microphone; (4) the light-absorbing sample; (5) a transparent window.

How this can be realized in practice is shown schematically in Fig. 3. It should be noted that in this configuration the system characteristics are identical in both cases and should disappear from the amplitude ratio

$$R(\omega) = q_r(\omega)/q_f(\omega) \tag{17}$$

and from the phase difference

$$\Delta\psi = \psi_f(\omega) - \psi_r(\omega) \tag{18}$$

One has the additional advantage that $g = b = e_g/e_s$, with e the thermal effusivity. Because of the Ti coating, one also has $\beta_s^{-1} \ll l_s$ and $r \gg 1$, resulting in $\exp(-\beta_s l_s) \simeq 0$ and $r \gg g$. All this results in a much simplified expression for Q of Eq. (3.5), namely,

$$Q = 2/(e^{\sigma_s l_s} + e^{-\sigma_s l_s}) \tag{19}$$

In Fig. 4, the R and $\Delta\psi$ results are given as a function of the modulation frequency. Although the effects of the system parameters have largely

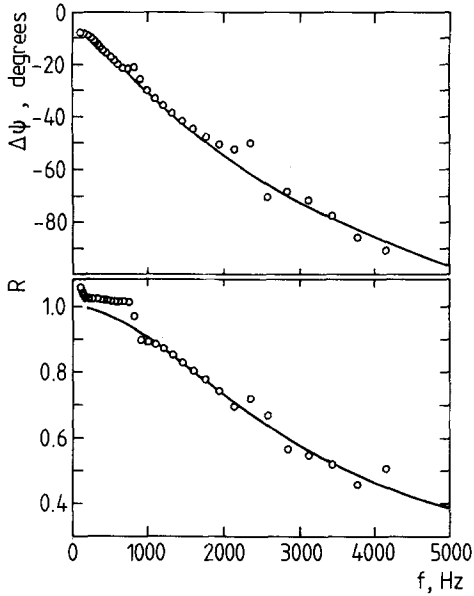

Fig. 4. Amplitude ratio R values and phase differences $\Delta\psi$ for a free-standing CVD diamond film from front and rear photoacoustic measurements in the configurations in Fig. 3. The solid curve is the result of a simultaneous nonlinear least-squares fit to the experimental data, resulting in a κ_s value of $(9.8 \pm 0.7) \times 10^2\ \mathrm{W \cdot m^{-1} \cdot K^{-1}}$.

been neutralized, there still is (near 800 Hz) a small effect of a cell resonance present. The solid curve in Fig. 4 is the result of a simultaneous nonlinear least-squares fitting [16, 21] of the R and $\Delta\psi$ data (excluding the data clearly affected by the spurious resonance). Fits have been carried out with Eq. (19) and with a slightly modified form, where, in the right-hand side of Eq. (19), a multiplicative factor $A_0 \exp(i\psi_0)$ was introduced. In the nonlinear least-square fits, in addition to the thermal diffusivity α, also A_0 and ψ_0 were adjustable parameters. This procedure was followed in order to allow for possible small differences in thermal wave production by illuminating the two different sides of the sample. From this kind of fit we obtained a value $\alpha = (5.5 \pm 0.4) \times 10^{-4}\,\mathrm{m^2 \cdot s^{-1}}$ with $A_0 = 1.09$ and $\psi_0 = 0.03$ rad. Including the data affected by the spurious cell resonance gave essentially the same result. Using literature values [22, 23] for the density and the heat capacity of natural diamond results, then, in a thermal conductivity value $\kappa = (9.8 \pm 0.7) \times 10^2\,\mathrm{W \cdot m^{-1} \cdot K^{-1}}$.

In order to verify the above result, another measuring configuration, given schematically in Fig. 5, was used, with a 64-μm-thick copper sheet as a reference material. In this case the ratio of the diamond and the copper rear signals was made. In Fig. 6 the phase difference as a function of the modulation frequency is compared with a simulation result (solid curve) calculated by means of Eq. (5) using the known thermal properties of copper [24] and the result for the CVD diamond film previously obtained with the setup in Fig. 3. In Fig. 6 good agreement can be observed.

3.2. Photothermal Beam-Deflection Measurements

In addition to the photoacoustic measurements, we also have carried out measurements on the same CVD film, by means of the photothermal beam deflection ("mirage" effect) detection technique schematically given in Fig. 2 and described in Section 2.2. Results for the amplitude and the phase

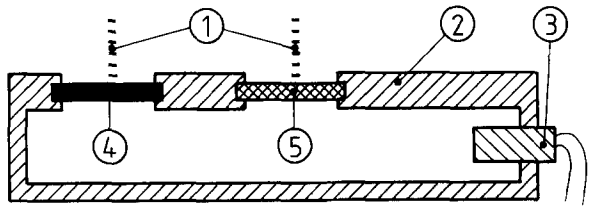

Fig. 5. Photoacoustic cell configuration for rear detection measurements on a free-standing CVD diamond film (4) and a reference copper sheat (5). (1) The modulated pump beam; (2) the cell body; (3) the microphone.

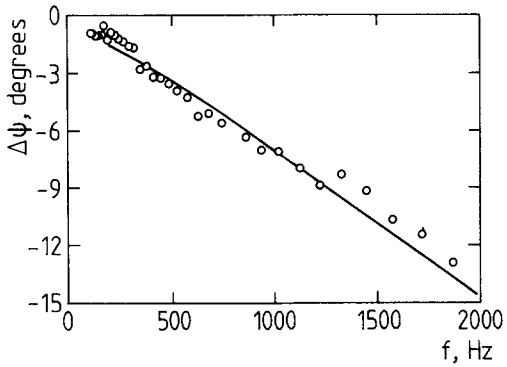

Fig. 6. Results for the phase differences $\Delta\psi$ obtained with the experimental setup in Fig. 5. The solid curve was calculated on the basis of the known thermal parameters of copper and the results for the CVD film with the front and rear configurations in Fig. 3.

of the normal component [Eq. (11)] of the probe beam deflection as a function of distance from the focussed pump beam are given, for three modulation frequencies: 40, 80, and 120 Hz. These experimental amplitude and phase results are compared with simulated results (solid curves) in Fig. 7.

For the purpose of this comparison, Eq. (11) was rewritten in the following form:

$$\varphi_n = A_0(\omega)\, e^{i\psi_0(\omega)} e^{i\omega t} \int_{y=-\infty}^{\infty} \frac{1}{\kappa_s} \dot{K}_0[(i\omega/\alpha_s)^{1/2} r]\, dy \tag{20}$$

In this way we replaced all the sample independent quantities in the prefactor of Eq. (11), as well as characteristics of the measuring system by a single adjustable amplitude factor $A_0(\omega)$ and phase shift $\psi_0(\omega)$ for each modulation frequency $f = \omega/2\pi$. This is a sensible approach because it would be very difficult to arrive at reliable absolute values for these quantities; e.g., z_0, appearing in $\exp(-\sigma_g z_0)$ of Eq. (11), is difficult to measure accurately. Moreover, only the thermal parameters κ_s and α_s are important for the shape of the amplitude and phase curves as a function of the distance from the pump beam, which is entirely contained in the integral part $I(\omega, r)$ of Eq. (20).

In Fig. 7, the solid amplitude and phase curves for three modulation frequencies represent $\kappa_s I(\omega, r)$ values calculated on the basis of the α_s and κ_s results obtained with the photoacoustic measurements described above. The experimental amplitude data of Fig. 7 are the experimental values

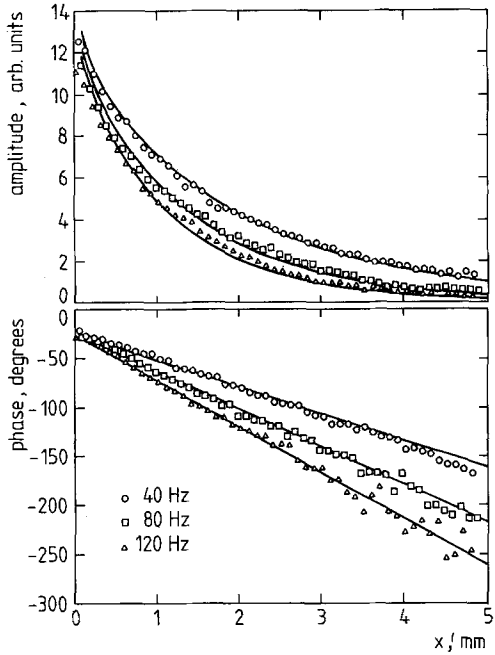

Fig. 7. Photothermal beam deflection results for the amplitude A and the phase ψ as a function of the distance x from the center of the pump beam focused at the surface of the CVD diamond film. Measurements have been carried out at three modulation frequencies: circles for $f = 40$ Hz, squares for $f = 80$ Hz, and triangles for $f = 120$ Hz. The solid curves are calculated using the results for the CVD film measured with the front and rear configurations in Fig. 3.

divided by an arbitrary factor $A'_0(\omega)$ formally corresponding to $A_0(\omega)/\kappa_s$. In a similar way the phase data have been arbitrarily shifted by $\psi'_0(\omega)/\kappa_s$. For all three modulation frequencies there is quite good agreement between the x dependence (determined by α_s) of the experimental and the calculated results.

The mirage data, thus, confirm the α_s value derived from the photoacoustic measurements. One should, however, realize that in the photoacoustic measurements, heat transport perpendicular to the surface was measured, while in the mirage measurements lateral heat transport in the film was considered. For our sample both values for α_s should be the same, as observed. This should not be the case anymore for anisotropic samples, but then it would be possible to study the anisotropy by combining this photoacoustic and the mirage techniques.

4. SUMMARY AND CONCLUSION

In this paper we have investigated heat conduction in a polycrystalline free-standing chemical vapor-deposited diamond film by means of different measuring techniques. As a first technique we used a new photoacoustic technique combining front and rear signal detection. In this approach there is no need for a reference material for the calibration of the photoacoustic cell. By this method we arrived at a value of $(5.5 \pm 0.4) \times 10^{-4}\ m^2 \cdot s^{-1}$ for the thermal diffusivity α_s of the CVD diamond film. Using literature values for the density and the heat capacity of natural diamond, a value of $(9.8 \pm 0.7) \times 10^2\ W \cdot m^{-1} \cdot K^{-1}$ for the thermal conductivity was obtained. This result was confirmed by using a different photoacoustic setup combining the rear signals for the CVD diamond films and a 64-μm-thick reference copper sheet. A photothermal beam deflection technique ("mirage" effect) was also used to measure lateral heat transport in the film. Good agreement was obtained with the result for the perpendicular heat conduction derived from the photoacoustic measurements, which is of course expected for our sample. A combination of our photoacoustic method and the mirage technique allows the measurement of thermal anisotropies. Our thermal conductivity value of $(9.8 \pm 0.7) \times 10^2\ W \cdot m^{-1} \cdot K^{-1}$ is also in very good agreement with a value of $960 \pm 60\ W \cdot m^{-1} \cdot K^{-1}$ obtained by Visser [25] by means of an infrared surface temperature scanning technique [6] for a sample of identical origin.

ACKNOWLEDGMENTS

We thank E. P. Visser for supplying us with the CVD diamond sample. We also like to thank the Research Council of the K. U. Leuven and the Belgian National Science Fund (NFWO) for financially supporting this work. W. Lauriks also thanks the Belgian National Science Fund (NFWO) for a Senior Research Assistantship.

REFERENCES

1. D. T. Morelli, C. P. Beetz, and T. A. Perry, *J. Appl. Phys.* **64**:3063 (1988).
2. A. Ono, T. Baba, H. Funamoto, and A. Nishikawa, *Jpn. J. Appl. Phys.* **25**:L803 (1986).
3. P. K. Kuo, L. Wei, and R. W. Prior, in *Proceedings of Symposium Q, 1989 Spring Meeting of the Materials Research Society*, R. H. Chang, D. Nelson, and A. Hiraka, eds. (Materials Research Society, Pittsburgh, 1989), p. 119.
4. P. K. Kuo, L. Wei, and R. L. Thomas, in *Photoacoustic and Photothermal Phenomena III*, D. Bicanic, ed. (Springer, Berlin, 1992), p. 175, 251.
5. S. Albin, W. P. Winfree, and B. Scott Crews, *J. Electrochem. Soc.* **137**:1973 (1990).
6. E. P. Visser, E. H. Versteegen, and W. J. P. van Enckevort, *J. Appl. Phys.* **71**:3238 (1992).

7. A. Rosencwaig, *Photoacoustics and Photoacoustic Spectroscopy* (John Wiley, New York, 1981).
8. C. Glorieux, E. Schoubs, and J. Thoen, *Mat. Sci. Eng.* **A112**:87 (1989).
9. J. Thoen, E. Schoubs, and V. Fagard, in *Physical Acoustics, Fundamentals and Applications*, O. Leroy and M. A. Breazeale, eds. (Plenum Press, New York, 1991), p. 179.
10. M. Müller, R. Osiander, A. Gold, and P. Korpiun, in *Photoacoustic and Photothermal Phenomena II*, M. C. Murphy, J. W. Maclachlan-Spicer, L. Aamodt, and B. S. H. Royce, eds. (Springer Verlag, Berlin, 1990), p. 198.
11. Z. Yasa and N. Amer, *Topical Meeting on Photoacoustic Spectroscopy*, Ames, Iowa (1979), paper WA5-1 (unpublished).
12. O. Pessoa, Jr., C. L. Cesar, N. A. Patel, H. Vargas, C. C. Ghizoni, and L. C. M. Miranda, *J. Appl. Phys.* **59**:1316 (1986).
13. F. A. McDonald and G. C. Wetsel, Jr., *J. Appl. Phys.* **49**:2313 (1978).
14. F. A. McDonald, *Am. J. Phys.* **48**:41 (1980).
15. A. Rosencwaig and A. Gersho, *J. Appl. Phys.* **47**:64 (1976).
16. C. Glorieux, J. Fivez, and J. Thoen, *J. Appl. Phys.* **73**:684 (1993).
17. A. C. Boccara, D. Fournier, and J. Badoz, *Appl. Phys. Lett.* **36**:130 (1980).
18. H. S. Carlslaw and J. C. Jaeger, *Conduction of Heat in Solids* (Oxford University Press, London, 1959).
19. J. C. Murphy and L. C. Aamodt, *J. Appl. Phys.* **51**:4580 (1980).
20. A. Salazar, A. Sànchez-Lavega, and J. Fernandez, *J. Appl. Phys.* **65**:4150 (1989).
21. P. R. Bevington, *Data Reduction and Error Analysis for the Physical Sciences* (McGraw–Hill, New York, 1969).
22. J. E. Field, *The Properties of Diamond* (Academic Press, London, 1979).
23. T. R. Anthony, W. F. Banholzer, J. F. Fleischer, Lanhia Wei, P. K. Kuo, R. L. Thomas, and R. W. Pryor, *Phys. Rev.* **B42**:1104 (1990).
24. R. C. Weast, ed., *Handbook of Chemistry and Physics*, 57th ed. (CRC, Cleveland, 1977).
25. E. P. Visser, private communications (1992).